# Wear numerical assessment for partial slip fretting fatigue conditions

R.A. Cardoso, T. Doca, David Néron, S. Pommier, J.A. Araújo

# Wear numerical assessment for partial slip fretting fatigue conditions

R.A. Cardoso[a,b,*], T. Doca[a], D. Néron[b], S. Pommier[b], J.A. Araújo[a]

[a] *Department of Mechanical Engineering, University of Brasilia, 70910-900 Brasilia, DF, Brazil*
[b] *LMT, ENS Paris-Sacaly, CNRS, Université Paris-Saclay, 61 avenue du Président Wilson, 94235 Cachan, France*

**Abstract**

The aim of this work is to evaluate wear effects on life prediction for components subjected to fretting conditions. Therefore, fretting fatigue FE simulations have been carried considering the geometry update due to the material removal and results were compared to both experimental data and FE simulations where wear was neglected. Well known multiaxial fatigue criteria in association with the Theory of Critical Distances (TCD) have been used to estimate life. Results have shown that, for the data assessed, where fretting fatigue tests were conducted on a Ti-6Al-4V alloy under partial slip conditions, considering wear effects might slightly increase the accuracy of life estimates. However, this improvement may not be worth the increase in the computational cost in such analysis.

*Keywords:* Fretting Fatigue, Wear, Multiaxial Fatigue, Theory of Critical Distances.

## Nomenclature

$a$: semi-width contact zone,
$A^s_{th}$: theoretical area of the slip zones,
$b'$: fatigue strength exponent,
$c$: semi-width contact stick zone,
$d'$: fatigue ductility exponent,
$E$: Young modulus,
$E_d$: friction energy dissipated during a fretting cycle,
$F_b$: bulk fatigue load applied to the rectangular specimen,
$h$: local wear depth,
$H$: hardness of the contacting surfaces,
$I_{FP}$: Findley multiaxial fatigue parameter,

*Corresponding author
*Email address:* rapha_2213@hotmail.com, araujo-cardoso@aluno.unb.br (R.A. Cardoso )

$I_{MWCM}$: Modified Wöhler Curve Method fatigue parameter,
$I_{SWT}$: Smith, Watson and Topper multiaxial fatigue parameter,
$K$: Archard's dimensionless wear coefficient,
$L$: critical distance,
$N_f$: number of cycles to failure,
$P$: normal force applied to the cylindrical pad,
$p_0$: contact peak pressure,
$Q$: fretting tangential force applied to the cylindrical pad,
$R_\sigma$: stress ratio,
$s$: local relative slip between contacting surfaces,
$S$: total relative slip between contacting surfaces,
$\underline{u}$: displacement field,
$u_x$: tangential displacement imposed on the cylindrical pad,
$V$: volume,
$\alpha$: energy wear coefficient,
$\Delta\varepsilon_n$: normal strain range,
$\gamma$: material parameter of Findley's multiaxial fatigue model,
$\kappa_w$: Archard's local wear coefficient,
$\kappa_\tau$: inverse of the slope of the modified Wöhler curves,
$\mu$: Coulomb friction coefficient,
$\nu$: Poisson's ratio,
$\rho$: multiaxial stress ratio,
$\underline{\underline{\sigma}}$: Cauchy stress tensor,
$\sigma_a$: stress amplitude,
$\sigma_b$: bulk stress,
$\sigma'_f$: fatigue strength coefficient,
$\sigma_m$: mean stress,
$\sigma_{n,\max}$: maximum normal stress,
$\sigma_{ut}$: ultimate stress,
$\sigma_y$: yield stress,
$\tau_a$: shear stress amplitude,
$\varepsilon'_f$: fatigue ductility coefficient,
FE: Finite Element,
FEM: Finite Element Method,
GSR: gross slip regime,
MRH: Maximum Rectangular Hull,
MSR: mixed slip regime,
MWCM: Modified Wöhler Curve Method,
PSR: partial slip regime,
SWT: Smith, Watson and Topper,
TCD: Theory of Critical Distances.

## 1. Introduction

Fretting takes place when two contacting parts are subjected to vibration loads which lead to a micro relative slip between them. This type of problem

commonly generates high levels of stress close to the contact surfaces favouring the nucleation of early cracks [1]. In addition, if one of the bodies is also subjected to cyclic fatigue loads, the so-called fretting fatigue phenomenon takes place. In this case, nucleated cracks may propagate at high rates resulting in catastrophic failures [2]. Fretting fatigue life prediction and crack arrest approaches generally neglect wear effects when partial slip conditions are predominant [3, 4, 5, 6, 7, 8]. However, the contact surface evolution due to wear, over the fretting cycles, may lead to appreciable changes in the stress field distributions caused by the contact loads [9, 10]. As most of the works done so far concerning life prediction for fretting problems rely on stress based models, considering wear effects may change life predictions. [11, 12] took into account wear effects in order to estimate fatigue life for a titanium alloy and could capture efficiently the detrimental wear effect under partial slip conditions and a beneficial one when gross sliding was observed. Under gross sliding conditions, cracks are worn out before they even start growing due to the high material loss. Besides, contact stress redistribution provides less severe sub-surface stress states. Argatov et al. [13] have used Archard's wear local law [9] in order to better understand wear degradation in wire ropes and highlighted some implications to fatigue life estimation. The fretting effect on fatigue life of thin steel wires was also investigated in [27] through a finite element wear model. This paper will focus on the analysis of fretting fatigue data undertaken at the University of Brasilia by [14, 15, 16] for the titanium alloy Ti-6Al-4V. The main idea here is to compare life predictions regarding wear effects with those obtained when wear is neglected. All the analyses are carried out under the partial slip regime (PSR).

This paper is divided as follows: in Section 2, some basic concepts about wear in the context of fretting fatigue are shown. In addition, the main ingredients for the simulation of wear as well as the evaluation of fatigue damage under fretting wear conditions are presented. In this section, two standard strategies for updating contact geometries are also compared (remeshing and adaptive meshing). In Section 3, the three different multiaxial fatigue criteria considered in this work are presented as well as the Theory of the Critical Distances (TCD), nonlocal approach commonly used to account the strong stress gradient inherent to contact problems. Experimental fretting fatigue data under partial slip conditions are given in Section 4. Section 5 presents the numerical model adopted in the present analysis. Calibration of the multiaxial fatigue criteria here assessed are shown in Section 6. Section 7 presents the methodology here adopted in order to estimate life either considering wear or neglecting it as well as the life estimate results and discussions. In the last section (Section 8), conclusions and remarks are expressed.

## 2. Wear modelling and damage accumulation

### *2.1. Wear aspects in the context of fretting fatigue*

Depending on the contact parameters, especially the slip amplitude, the fretting process can be divided into three different regimes [17], namely partial

slip regime (PSR), gross slip regime (GSR) and the so-called mixed slip regime (MSR). Regarding the PSR, the main mechanics of failure is fretting fatigue, where in this case the contact region is divided into slip and stick zones and the wear process is considerably small and confined to the slip areas. On the other hand, fretting wear is dominant in GSR, where in this case, crack growth is limited by the considerably high material removal. The MSR is observed for intermediate slip ranges and it inherits characteristics from both PSR and GSR. In [18] the MSR is reported to be the most dangerous regime for crack nucleation and progation. The effect of slip amplitude can be qualitatively extracted through fretting maps as the famous one presented by Vingsbo and Söderberg [19].

During fretting, wear is inherent to the problem, influencing the nucleation and propagation of cracks. Recent studies [11, 12, 20] have taken into account this issue by developing a coupled wear and fatigue approach. The simulation of material removal is addressed by using local formulations of Archad's equation [9, 10] or the dissipated friction energy [21, 22].

Archad's equation for sliding wear is commonly expressed as [23]:

$$\frac{V}{S} = K\frac{P}{H} \tag{1}$$

where $K$ is the dimensionless wear coefficient and $H$ is the material hardness. $P$, $S$ and $V$ are the normal contact load, total relative slip and volume of material removed, respectively. Considering an infinitesimal area, Eq. (1) can be expressed locally as:

$$dh = \kappa_w p ds \tag{2}$$

where $dh$ is the material removal depth for a given incremental relative slip $ds$, $p$ is contact pressure and $\kappa_w$ the local wear coefficient.

On the other hand, the friction energy wear law consists in relating the total wear volume to the accumulated friction energy dissipated on the contact interface.

$$V = \alpha \sum E_d \tag{3}$$

where $E_d$ is the friction energy dissipated during a fretting cycle and $\alpha$ is the energy wear coefficient. Locally, for an infinitesimal area, the wear depth can the be expressed by

$$dh = \alpha q ds \tag{4}$$

where $q$ is the contact shear traction.

Equations (2) and (4) implemented incrementally in a nodal basis through finite element simulations could provide a better understanding of the slip regimes influence on fretting fatigue behaviour, where in general, under gross slip conditions, wear has beneficial effects once it removes severely damaged areas before cracks start propagating. On the contrary, under partial slip regimes, wear tends to increase the damage process and at the same time it shifts the crack initiation sites towards the stick/slip transition regions [9, 10, 11, 12, 20].

*2.2. Numerical modelling and damage accumulation*

As presented in Section 2.1, wear can be computed locally by using the Archard's law, Eq. (2) or the dissipated friction energy local law, Eq. (4). Those equations can be readily implemented in the context of a FE code. In this setting, the total required number of wear cycles (loading cycles), $N_t$, can be split in $n_w$ wear blocks, where each block corresponds to $\Delta N$ wear cycles, i.e. $n_w = N_t/\Delta N$. From a practical point of view, it would not be feasible in many situations to simulate each wear cycle. In this case, a strategy commonly adopted is to compute the wear during a fretting cycle and then multiply it by the jumping factor $\Delta N$ assuming that the wear is nearly constant for $\Delta N$ wear cycles. Doing so, the contact surface of the problem can be updated on a nodal basis after the application of the $i^{th}$ wear block $\Delta N$ as follows:

- Archard's law:

$$\Delta h_{i,j} = \sum_{k=1}^{n_{inc}} \kappa_w p(x_j, t_k) \Delta s(x_j, t_k) \Delta N \tag{5}$$

- Frictional dissipated energy:

$$\Delta h_{i,j} = \sum_{k=1}^{n_{inc}} \alpha q(x_j, t_k) \Delta s(x_j, t_k) \Delta N \tag{6}$$

where $\Delta h_{i,j}$ is the wear depth increment of the node $j$ located at the contact surface with position $x_j$, $\kappa_w$ is the local wear coefficient, $\alpha$ is the energy wear coefficient and $n_{inc}$ is the total number of load increments over a fretting cycle. The contact variables $p(x_j, t_k)$, $q(x_j, t_k)$ and $\Delta s(x_j, t_k)$ denote, respectively, the pressure distribution, the shear traction and the contact relative slip increment for the node $j$ at the time increment $t_k$. Therefore, the total wear depth at $N_t$ cycles for the node $j$ is given by:

$$h_j = \sum_{i=1}^{n_w} \Delta h_{i,j} \tag{7}$$

Besides the update of the contact surface, which is addressed in the next section, changes in stress and strain are recorded for each wear step so that the Miner's linear cumulative damage rule [24, 25] can be used to predict material failure. In this case, for a material sub-surface point $\underline{x}$, the total cumulative damage associated with the $n^{th}$ wear step is given by:

$$D_{f,n}(\underline{x}) = \sum_{i=1}^{n} \frac{\Delta N}{N_{f,i}(\underline{x})} \tag{8}$$

where $N_{f,i}$ is the fatigue life expected for a given stress state, i.e. after determining the stress state $\underline{\underline{\sigma}}(\underline{x}, t)$ for given material point $\underline{x}$ and time instant $t$ over

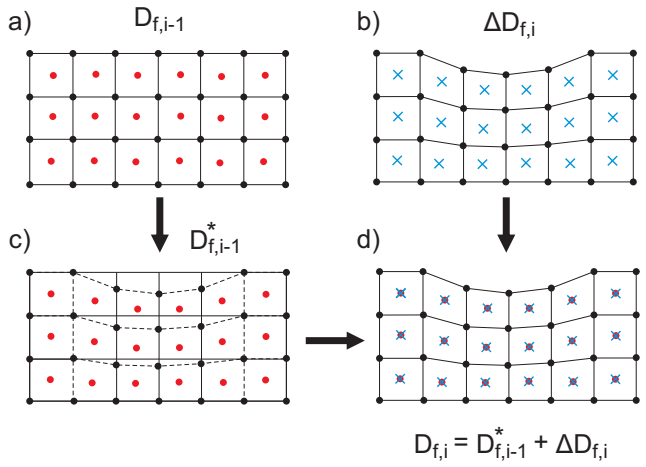


Figure 1: Illustration of the methodology used in order to accumulate damage when considering wear: (a) accumulated damage at the centroid of the elements at the $(i-1)^{th}$ simulated fretting cycle, (b) incremental damage at the centroid of the elements at the $i^{th}$ simulated fretting cycle, (c) accumulated damage at the $(i-1)^{th}$ simulated fretting cycle extrapolated to the position of the element centroids at the $i^{th}$ simulated fretting cycle and (d) accumulation of the total damage at the $i^{th}$ simulated fretting cycle.

the $i_{th}$ fretting cycle, it can be introduced in multiaxial fatigue criteria in order to predict the fatigue life $N_{f,i}(\underline{x})$ (see Section 3).

In this work, the centroid of elements were chosen in order to compute the damage parameter defined by Eq. (8). However, it is worth noting that, due to the material removal along the contact surfaces, the contact geometries are constantly modified which as consequence changes the position of the element centroids describing such geometries (mainly under gross sliding conditions). In order to account for that, the following numerical scheme was adopted: after each $i^{th}$ fretting cycle simulation, the damage value on the $(i-1)^{th}$ fretting cycle was interpolated from the $(i-1)^{th}$ element centroids position to the new $i^{th}$ element centroids location. Therefore, the actual damage field distribution at the $i^{th}$ damage increment can be expressed as:

$$D_{f,i} = D^{\star}_{f,i-1} + \Delta D_{f,i} \tag{9}$$

where $D^{\star}_{f,i-1}$ is the damage field from the previous fretting cycle simulation $(i-1)^{th}$ interpolated to the position of the element centroid points at the $i^{th}$ fretting cycle, Figure 1. As can be seen, this strategy ensures that damage is not accumulated at material points removed due to wear. Damage interpolation from a previous mesh configuration ($D_{f,i-1}$) to the new one ($D^{\star}_{f,i-1}$) were performed by firstly applying a Delaunay triangulation to points at the $(i-1)^{th}$ centroids location followed by a linear interpolation of $D_{f,i-1}$ to the new element centroid positions.

### 2.3. Contact surface update

In order to update the contact surfaces as the fretting cycles goes on, two different strategies are commonly applied. One of them is the remeshing technique [9, 10, 20], in this case, after the simulation of a fretting cycle, the coordinates of the contact nodes are vertically displaced by the amount defined in Eqs. (5)-(6) and another mesh is generated in order to avoid element distortion. Another way to tackle the problem is by using adaptive meshes [11, 26, 27, 28], where the position of the contact nodes are also displaced over the fretting cycles, however, this technique dispenses the remeshing procedure once the mesh topology is held the same while nodal positions are shifted in order to avoid distortion. However, an advection process needs to be carried out, which consists in remapping solution variables from an old mesh to the new one.

These two techniques were implemented and tested in this work by usig the commercial FE software ABAQUS 6.14 [29]. For more details concerning their implementation and numerical issues see Appendix A. Briefly speaking, the adaptive meshing technique was computationally more efficient than the remeshing technique, however, for partial slip conditions, the adaptive meshing procedure did not provide a clear stabilization of the contacting surfaces profile, which lead to overestimate wear effects. In addition, it is very memory demanding. In this setting, as this work is settled in the context of high cycle fatigue under PSR, the remeshing technique was adopted.

## 3. Multiaxial Fatigue

Most of the experimental data available, even today, consists of tests performed under uniaxial stress or pure torsional conditions. However, for fretting applications, multiaxial stress states are much more likely to happen. In this case, it is often unrealistic the idea of reproducing experimentally the load conditions observed in real components experiencing service conditions. The basic idea behind the multiaxial fatigue criteria is to use data provided from simple laboratory tests in order to design against multiaxial and more complex stress states. In this work, three different multiaxial fatigue models based on critical plane approaches are considered.

### 3.1. Findley Model

After analyse an extensive amount of experiments, for instance the ones carried out by [31, 32], Findley [33] has proposed the following multiaxial fatigue damage parameter:

$$I_{FP} = (\tau_a + \gamma \sigma_{n,\max})_{\max} \tag{10}$$

where $\gamma$ is a material parameter. $\tau_a$ and $\sigma_{n,\max}$ are the shear stress amplitude and the maximum normal stress, respectively, for a given material plane. The idea behind this model is that shear stresses lead to crack nucleation and early propagation whereas normal stress increases crack opening and consequently rate of growth. For ductile materials $\gamma$ ranges between 0.2 and 0.3 and it can

be obtained considering the results of fatigue tests performed on different stress states.

### *3.2. Smith, Watson and Topper (SWT) Model*

An alternate model is necessary for materials that fail predominately by crack growth on planes of maximum tensile strain or stress. In these materials, despite the fact that cracks still nucleates under shear mode, crack growth takes place on planes perpendicular to maximum principal stress and strain. In their model, [34] proposed a relationship that takes into account both cyclic strain range and maximum normal stress.

$$I_{SWT} = \sigma_{n,\max} \frac{\Delta\varepsilon_n}{2} \tag{11}$$

where $\sigma_{n,\max}$ and $\Delta\varepsilon_n$ are the maximum normal stress and normal strain range on the material plane that maximizes their product. This model can also handle non-proportional loading conditions. It also permits to estimate the component life by reference to a fully reversed uniaxial test where Basquin (stress-life) and Coffin Manson (strain-life) relations can be combined yielding:

$$\sigma_{n,\max} \frac{\Delta\varepsilon_n}{2} = \frac{(\sigma_f'^{\,2})}{E} (2N_f)^{b'} + \sigma_f' \varepsilon_f' (2N_f)^{b'+d'} \tag{12}$$

where $\sigma_f'$ and $\epsilon_f'$ are the fatigue strength and ductility coefficients, respectively, while $b'$ and $d'$ are the fatigue strength and ductility exponents, respectively.

### *3.3. Modified Wöhler Curve Method (MWCM)*

Based on the theory of cyclic deformation in single crystals, which suggests that fatigue damage in polycrystals depends on the maximum shear stress amplitude and stress component normal to the crack initiation plane, [35] proposed their model.

Considering the assumption that cracks nucleates on planes experiencing maximum shear stress amplitude, the critical plane can be defined as the material plane subjected to the maximum shear stress amplitude $\tau_a$ over a loading cycle. Regarding this plane, it is also possible to define the following stress ratio:

$$\rho = \frac{\sigma_{n,\max}}{\tau_a} \tag{13}$$

where $\sigma_{n,\max}$ is the maximum normal stress developed at the critical plane. Note that this term accounts the influence of mean stress on multiaxial fatigue strength. Without further ado, the idea of the MWCM consists in characterizing the conventional S-N curves however assessing $\tau_a$ vs $N_f$, [35]. As well as the presence of mean stress modifies S-N curves, the stress ratio $\rho$ alters the Modified Wöhler curves, Figure 2, where $\tau_{a,ref}$ is defined as the shear stress amplitude at a certain number of cycles to failure $N_{ref}$ and $\kappa_\tau$ is the inverse slope of the

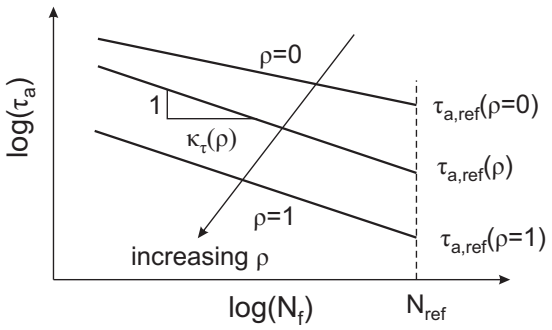


Figure 2: Modified Wöhler curves.

curve $\log(N_f)$ vs. $\log(\tau_a)$. Therefore, for a generic stress ratio $\rho$ and shear stress amplitude $\tau_a$, the fatigue life may be estimated through the following relation:

$$N_f = N_{ref} \left[ \frac{\tau_{a,ref}(\rho)}{\tau_a} \right]^{\kappa_\tau(\rho)} \tag{14}$$

where $\tau_{a,ref}(\rho)$ and $\kappa_\tau(\rho)$ can be obtained through linear interpolation considering data from two different experiment campaigns. For example, considering fully reversed uniaxial ($\rho = 1$) and torsional ($\rho = 0$) fatigue curves one has:

$$\tau_{a,ref}(\rho) = [\tau_{a,ref}(\rho = 1) - \tau_{a,ref}(\rho = 0)]\rho + \tau_{a,ref}(\rho = 0) \tag{15}$$

and

$$\kappa_\tau(\rho) = [\kappa_\tau(\rho = 1) - \kappa_\tau(\rho = 0)]\rho + \kappa_\tau(\rho = 0) \tag{16}$$

When reference shear stress values correspond to fatigue limits, Eq. (15) becomes:

$$\tau_a + \left( \tau_{-1} - \frac{\sigma_{-1}}{2} \right) \frac{\sigma_{n,\max}}{\tau_a} \leqslant \tau_{-1} \tag{17}$$

It is worth mentioning that the use of the MWCM for large values of $\rho$ leads to conservative results. It can be explained by the fact that, once the mean normal stress on the critical plane is larger than a certain value, micro/meso cracks are completely open and thus shear forces are completely transmitted to the crack tips instead of being partially supported by the friction interactions between cracks faces [36, 37]. Therefore, the MWCM formulation is valid as long as $\rho$ is lower than a threshold value $\rho_{crit}$, where its expression is given by [38]:

$$\rho_{crit} = \frac{\tau_{-1}}{2\tau_{-1} - \sigma_{-1}} \tag{18}$$

where whenever $\rho \geqslant \rho_{crit}$ it can be set to $\rho_{crit}$.

### 3.4. Theory of critical distances (TCD)

It is well known that hot-spot approaches lead to very conservative results when high stress gradients are present like the ones found close to notches and the edges of contact problems. The theory of critical distances (TCD) was first proposed in order to deal with problems in presence of stress raisers such as notches and cracks [39]. In its most fundamental definition, the idea consists in evaluating an effective stress $F(\underline{\underline{\sigma}})$ that can appropriately characterize the fatigue damage process inside a specified volume $V$ surrounding the stress raiser:

$$\frac{1}{V}\int_V F\left(\underline{\underline{\sigma}}\right) dV \leqslant b \tag{19}$$

where $b$ is a material property associated with its fatigue strength. The volume $V$, in general is associated with the material characteristic length $L$, a material property that can be defined as [40]:

$$L = \frac{1}{\pi}\left(\frac{\Delta K_{th}}{\Delta \sigma_{-1}}\right)^2 \tag{20}$$

where $\Delta K_{th}$ is the material threshold stress intensity factor range and $\Delta\sigma_{-1}$ is the uniaxial fatigue limit range. For 2D analysis, the TCD can be expressed in its simplified versions (Figure 3) by substituting the material volume mentioned above by a point, line or area, respectively, with $\underline{\underline{\sigma}}(r,\theta)$ defined in polar coordinates:

- Point method

$$F\left(\underline{\underline{\sigma}}(L/2,0)\right) \leqslant b \tag{21}$$

- Line method

$$\frac{1}{2L}\int_0^{2L} F\left(\underline{\underline{\sigma}}(r,0)\right) dr \leqslant b \tag{22}$$

- Area method

$$\frac{2}{\pi L^2}\int_{-\pi/2}^{\pi/2}\int_0^{L} F\left(\underline{\underline{\sigma}}(r,\theta)\right) r dr d\theta \leqslant b \tag{23}$$

One of the main advantages of the TCD is that it can be used in conjunction with any multiaxial fatigue criteria [41].

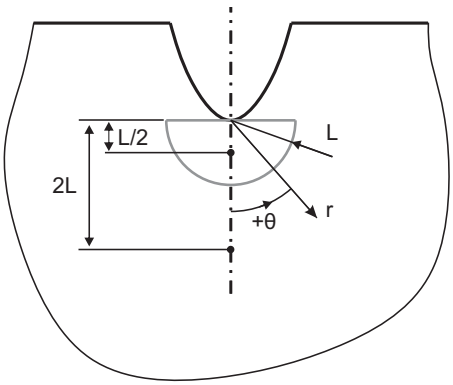


Figure 3: TCD averaging regions in its simplified 2D versions (point,line and area).

## 4. Experimental data

Aiming to investigate the influence of wear under fretting fatigue conditions (partial slip), the experimental data provided by [14, 16] is assessed and used as reference for comparison with the numerical results. In her work, besides evaluating the applicability of the nonlocal intensity factors proposed by [42] when those are used to define crack initiation frontiers under fretting conditions, the size effect in fretting fatigue problems was also investigated. In this case, two types of experimental campaigns were evaluated. In one of them (Group-2a of tests) [1], the aim was to investigate the effect of the volume of material being stressed under the contact. In this group-2a tests, the stress gradient inward the contact and the area of the slip zones were the same for all the experiments. In the other set of experiments (Group-2b of tests), the goal was to verify the influence of damaged area on the tests while the stress gradient was kept the same. The contact geometry considered was the cylinder on plane one. For more details concerning pads and specimens manufacturing and specifications, see [14].

The stress gradient inward the contact moving away from the trailing edge was evaluated via the MWCM (see Subsection 3.3).

The data provided by [14, 16] is presented in Table 1, where $\sigma_{b,max}$ is the maximum value reached by the bulk stress during a fretting cycle while $Q_{max}$ is the maximum tangential load. $A^s_{th}$ is the theoretical area of the slip zones and $N_f^{exp}$ is the experimental number of cycles to failure. A pad radius $R = 70$ mm was considered in the analysis. A peak pressure $p_0 = 500$ MPa was kept in all tests. The numerical model and load sequence considered in the experiments

[1] The nomenclature Group-2a is here used in order to be in accordance with the one utilized in [14, 16], where, in her work, Group-1 tests were intended to verify the accuracy of the nonlocal intensity factors presented by [42] in estimating fretting crack initiation frontiers.

Table 1: Group-2 fretting fatigue data for the Ti-6Al-4V [14, 16] (pad radius $R = 70$ mm).

| test | thickness (mm) | $\sigma_{b,max}/p_0$ | $Q_{max}/\mu P$ | $A^s_{th}$ (mm$^2$) | $N_f^{exp}$ |
|---|---|---|---|---|---|
| T1 | 8 | 0.45 | 0.68 | 7.43 | 218000 |
| T2 | 13 | 0.6 | 0.46 | 7.37 | 167000 |
| T3 | 8 | 0.3 | 0.65 | 7.01 | 672000 |
| T4 | 13 | 0.46 | 0.44 | 6.99 | 443000 |
| T5 | 8 | 0.6 | 0.46 | 4.53 | 207000 |
| T6 | 8 | 0.40 | 0.42 | 4.08 | 529000 |
| T7 | 13 | 0.40 | 0.42 | 6.62 | 538000 |

Table 2: Mechanical properties of the Ti-6Al-4V alloy [44].

| Material | $E$ (GPa) | $\nu$ | $\sigma_y$ (MPa) | $\sigma_{ut}$ (MPa) | $HV$ |
|---|---|---|---|---|---|
| Ti-6Al-4V | 119.4 | 0.286 | 850 | 1000 | 360 |

are depicted in Figure 5, where more details will be given in Section 5. Tests from 1 to 4 aimed to investigate the effect of the volume of material being stressed. For example, tests T1 and T2 were designed to have the same slip areas (Figure 4(a)) and the same stress gradient at the contact trailing edge ($x = -a$), however with different volumes of material being stressed. This can be done by changing the specimens and pads thickness, i.e. from 8 to 13 mm. In order to keep the same slip areas between these two tests, the tangential load needs to de modified, once it changes the length of the slip areas. Doing so, the bulk load also needs to be adequately changed in order to hold the same stress gradient for the two tests (T1 and T2). Same is required for tests T3 and T4, however in this case, loads are lower so that higher lives could be achieved during experiments.

On the other hand, tests T2, T5-T7 were intended to investigate the influence of the damaged area due to wear on fretting fatigue, Figure 4(b). In this setting, tests T2 and T5 have the same stress gradient nearby the contact edges, however, the size of the slip areas are different within these two tests. The same is valid for tests T6 and T7 but with a less severe stress gradient.

All these experiments were conducted in the facilities of the Fatigue, Fracture and Materials Research Group at the University of Brasilia. The material of the pads and specimens was the titanium alloy Ti-6Al-4V. Its basic properties are given in Table 2. The friction coefficient, $\mu$, is 0.5 [43].

## 5. Numerical model

To carry out the fretting fatigue simulations, the commercial FE software ABAQUS 6.14 was used [29]. It allowed a faster and simpler implementation of

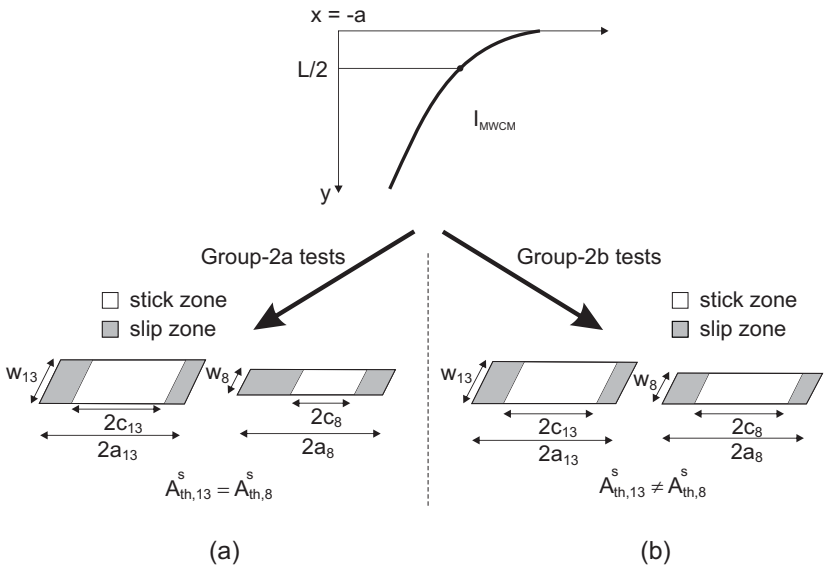


Figure 4: Schematic representation of the Group-2 tests: (a) Group-2a tests with the same slip zone areas for different contact widths, (b) Group-2b tests with different slip zone areas.

the contact evolution approach assessed in this work. The FE model adopted in this work is illustrated in Figure 5. As depicted, a static normal load, $P$, presses a cylindrical pad of radius $R$ against a flat specimen which is already subjected to a static mean bulk load, $F_b$. After that, a tangential load $Q$ is applied to the pad in phase with an alternate bulk load. Note that the mean and the alternate bulk loads give rise to the mean ($\sigma_m$) and alternate ($\sigma_a$) bulk stresses, respectively. A central refined zone composed of linear quadrilateral elements is defined in a rectangular region surrounding the contact surfaces. The size of the elements in this area is around 15 $\mu$m, which ensured a good compromise between stress solutions accuracy and computational cost. Outside this region, a coarser mesh is formed by linear triangular elements. Plane strain elements are considered in the analysis. Concerning the contact aspects, the nodes on the refined region of the pad are defined as the slave ones while the master nodes are set on the specimen. The frictional contact constraints are imposed via the Lagrange multiplier approach. The penalty method was not used here once that, in order to perform wear computations, exact slip solutions are needed inside the stick zones (the Penalty method allows some slip to take place even under stick conditions). Multi-point constraints are enforced on the upper surface of the pad so that rotation is prevented.

To validate the FE model, a fretting fatigue problem neglecting wear effects was simulated and results were compared to the analytical solution of the problem [45, 46, 47]. Figure 6 depicts the normal and shear traction distributions along the contact when both the tangential and the bulk loads achieve their

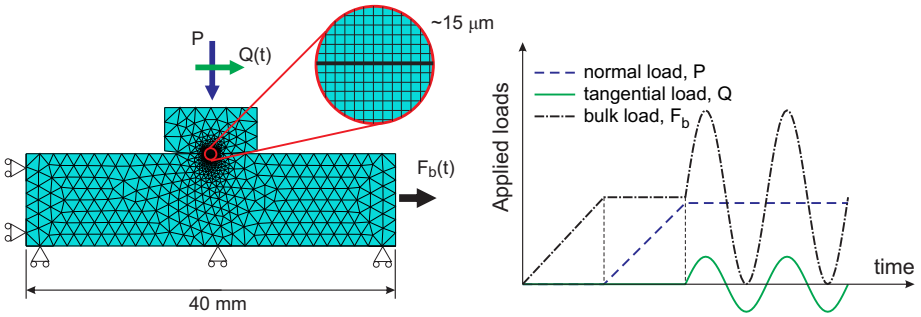


Figure 5: Finite element model used in order to carry out fretting fatigue/wear simulations.

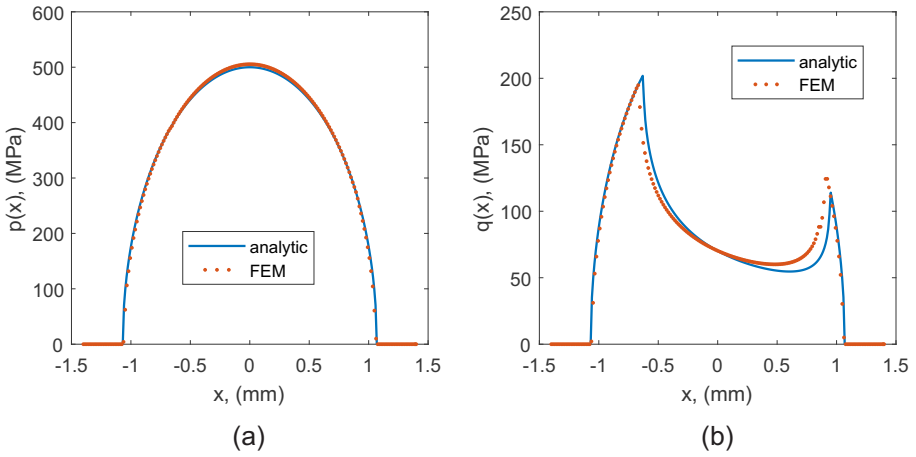


Figure 6: Comparison between analytical and FE solution: (a) pressure and (b) shear traction distribution (loading conditions from test T2 in Table 1).

maximum value (load case test T2). As can be seen, a good agreement can be found between the FE predictions and analytical solution of the problem.

## 6. Multiaxial fatigue life assessment

The main objective of this work is to investigate the effects of wear when estimating fatigue life under fretting conditions. The material investigated here is the Ti-6Al-4V. To calibrate the fatigue models presented in Subsection 3, the uniaxial fatigue data provided by [48] was used, see Figure 7. In this case, S-N curves for the Ti-6Al-4V were obtained considering uniaxial tests for different load ratios $R_\sigma$.

For instance, when considering the Smith, Watson and Topper (SWT) fatigue model, the fatigue data presented in Figure 7 can be expressed by means

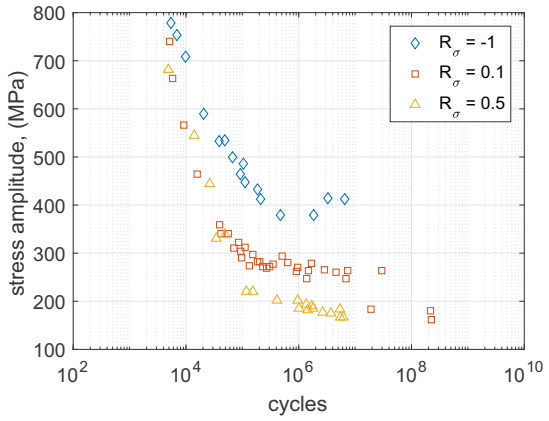


Figure 7: Uniaxial fatigue data for the Ti-6Al-4V [48].

of its parameter, Eq. (11), as a function of the number of cycles to failure, Figure 8. Then, a four-parameter power law can be used to fit the experimental data yielding:

$$I_{SWT} = 4.35N_f^{-0.093} + 2.45 \times 10^4 N_f^{-0.94} \tag{24}$$

Figure 9 illustrates the same procedure previously described, however using Findley's multiaxial fatigue parameter, which produces:

$$I_{FP} = 1.02 \times 10^5 N_f^{-0.64} + 363N_f^{-0.031} \tag{25}$$

Note that the computation of $I_{FP}$ demands the knowledge of the material parameter $\gamma$ (see Eq. (10)), which for metals, in general, ranges between 0.2 and 0.3. The value value of 0.3 was assumed in this work.

Finally, considering the Modified Wöhler Curve Method (MWCM), the following expressions were found:

$$N_f = 5 \times 10^6 \left[\frac{\tau_{a,ref}(\rho)}{\tau_a}\right]^{\kappa_\tau(\rho)} \tag{26}$$

where

$$\tau_{a,ref}(\rho) = -32\rho + 205 \tag{27}$$

and

$$\kappa_\tau(\rho) = -0.0269\rho - 0.0711 \tag{28}$$

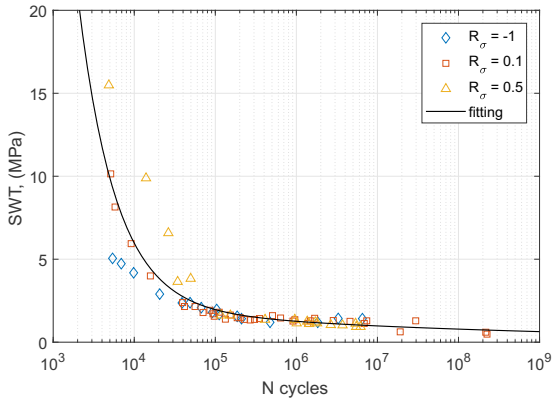


Figure 8: Uniaxial fatigue data for the Ti-6Al-4V [48] expressed in terms of the SWT parameter.

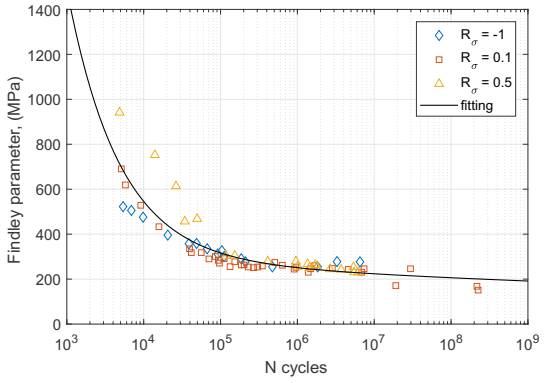


Figure 9: Uniaxial fatigue data for the Ti-6Al-4V [48] expressed in terms of the Findley parameter.

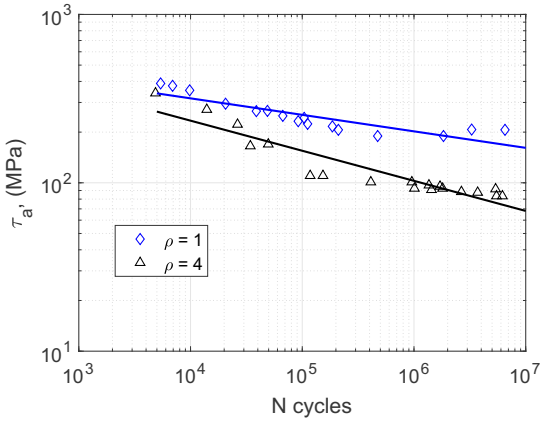


Figure 10: Uniaxial fatigue data for the Ti-6Al-4V [48] expressed in terms of the MWCM.

In order to obtain Eqs. (27) and (28) the interpolation strategy shown in Subsection 3.3 was applied to the uniaxial fatigue data corresponding to the load ratios $-1$ ($\rho = 1$) and 0.5 ($\rho = 4$). Figure 10 depicts the two reference modified Wöhler curves investigated. In order to compute $\tau_a$ used in the Findley and MWCM multiaxial fatigue criteria, the Maximum Rectangular Hull (MRH) has been used [49]. Note that these three multiaxial fatigue models considered presented a considerable dispersion for low cycle fatigue data. However, for high cycle fatigue, the regime assessed in this work, correlation with uniaxial data is quite fair.

Again, as this work aims to check if it is really worthwhile considering wear effects under partial slip conditions, three different models are used in an attempt to minimize the influence of the multiaxial fatigue criteria considered in the present investigation.

## 7. Results

Aiming to investigate the effects of wear under fretting fatigue conditions, two types of simulations were performed in this work. Firstly, wear effects were neglected in order to estimate fatigue life. In sequence, wear effects were considered following the procedures described in the previous sections. The friction dissipated energy equation (Eq. (6)) was considered in the analysis due to experimental availability of the energy wear coefficient $\alpha$ for the Ti-6Al-4V, which was obtained from [20], ($\alpha = 1.43 \times 10^{-8}$ MPa$^{-1}$).

Figure 11 depicts the worn surface of the specimen for different number of cycles when the load conditions given by the test T1 are considered. Contact pressure distribution for different number of cycles are shown in Figure 12(a). On the other hand, Figure 12(b) depicts the shear traction distribution over the cycles. Pressure profiles are taken before applying the tangential load, i.e.

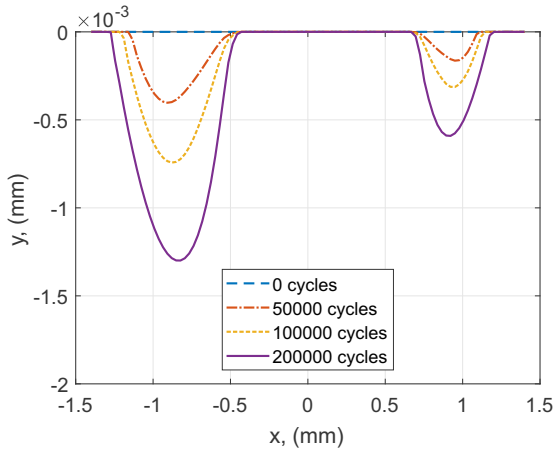


Figure 11: Specimen's predicted worn profile for different number of fretting fatigue cycles considering loading conditions from test T1.

$Q(t) = 0$, whereas shear tractions are obtained when $Q(t) = Q_{max}$. As can be seen, the presence of the bulk load $F_b$, besides provoking an offset of the stick zone, makes the material removal more prominent on the left slip zone. As fretting cycles goes on, pressure distributions on the initial slip zones are reduced while stress distributions at the initial stick zones are increased in order to keep the force equilibrium. Peaks in the transitions between stick and slip zones are also observed. A similar trend is observed when loading conditions from the other tests (Table 1) are assessed.

Fatigue life was estimated by using each one of the three different multiaixal fatigue criteria given by Eqs. (24)-(26). Note that when wear is included in the analysis, the damage cumulation law presented in Subsection 2.2 is needed once, due to the material removal and geometry modification, stress distributions are constantly changing. Since hot spot approaches are not well suited for contact problems [3, 50, 51], a nonlocal procedure based on the Theory of Critical Distances (point method) have been used in this work (see Subsection 3.4 for more details). A critical distance parameter $L = 30$ $\mu$m was adopted in this work [43].

When neglecting wear effects, stresses/strains can be readily obtained considering a point $L/2$ vertically distant from the contact trailing edge and life can be estimated through multiaxial fatigue criteria, Figure 13. However, when wear takes place, the hot spot point at the contact surface is continually changing. In this case, in order to estimate fatigue life, the procedure adopted here is to compute the damage parameter defined by Eq. (8) and check when it achieves the value of 1 (failure). However, failure is only considered when this point is at least $L/2$ distant from the contact surface, Figure 14. This procedure was conducted in order to incorporate the stress gradient in the life estimation

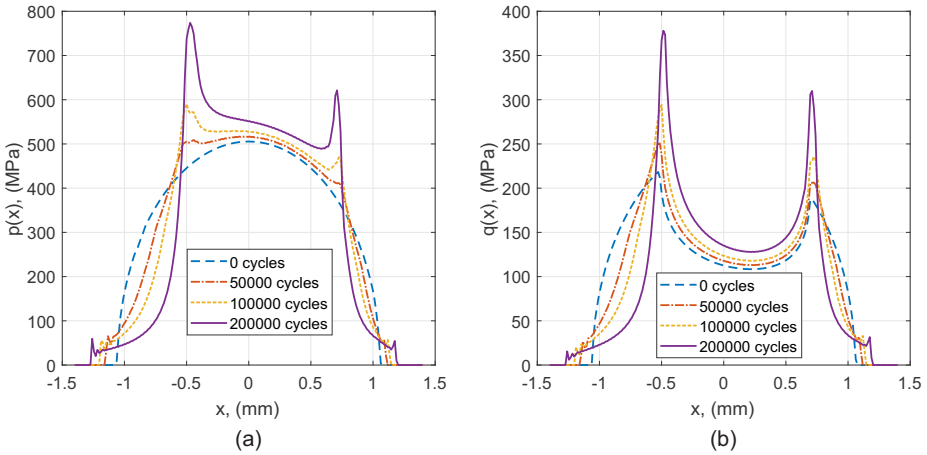


Figure 12: Contact traction distribution for different number of fretting fatigue cycles considering loading conditions from test T1: (a) pressure ($Q(t) = 0$) and (b) shear traction ($Q(t) = Q_{max}$).

procedure. If stresses were considered too close from the contact surface, life estimates would be systematically underestimated.

Table 3 summarizes the life estimate for the experimental data presented in Table 1 when wear effects are taken into account. Life results are provided considering each one of the multiaxial fatigue criteria presented in Section 6, i.e. SWT ($N_f^{SWT}$), Findley ($N_f^{FP}$) and MWCM ($N_f^{MWCM}$). The same is valid for Table 4 but neglecting wear effects, i.e. contact geometry is assumed to be the same all over the fretting cycles.

Note that tests conduced at the same loading levels but with different specimen thickness presented the same life estimates (T2/T5 and T6/T7). This is due to the fact that one carries out numerical simulations by assuming 2D

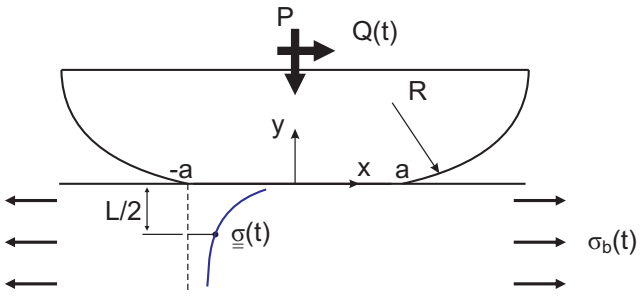


Figure 13: TCD applied to fretting problems when wear effects are neglected.

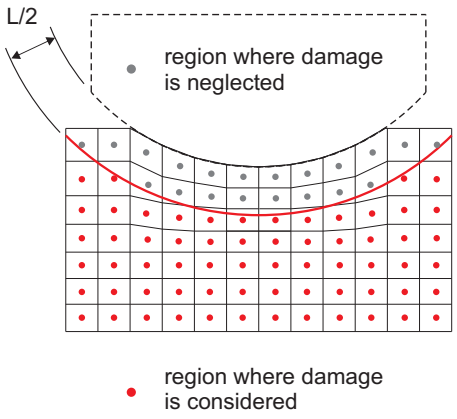


Figure 14: TCD applied to fretting problems when wear is taken into account.

Table 3: Life estimates condidering wear effects.

| **Results considering wear** | | | | |
|---|---|---|---|---|
| test | $N_f^{exp}$ | $N_f^{SWT}$ | $N_f^{FP}$ | $N_f^{MWCM}$ |
| T1 | 218000 | 271000 | 155000 | 132000 |
| T2 | 167000 | 304000 | 174000 | 208000 |
| T3 | 672000 | 405000 | 251000 | 192000 |
| T4 | 443000 | 573000 | 328000 | 343000 |
| T5 | 207000 | 304000 | 174000 | 208000 |
| T6 | 529000 | 821000 | 447000 | 475000 |
| T7 | 538000 | 821000 | 447000 | 475000 |

Table 4: Life estimates neglecting wear effects.

| **Results neglecting wear** | | | | |
|---|---|---|---|---|
| test | $N_f^{exp}$ | $N_f^{SWT}$ | $N_f^{FP}$ | $N_f^{MWCM}$ |
| T1 | 218000 | 106000 | 75000 | 152000 |
| T2 | 167000 | 122000 | 87000 | 237000 |
| T3 | 672000 | 387000 | 187000 | 512000 |
| T4 | 443000 | 452000 | 224000 | 733000 |
| T5 | 207000 | 122000 | 87000 | 237000 |
| T6 | 529000 | 1363000 | 465000 | 1441000 |
| T7 | 538000 | 1363000 | 465000 | 1441000 |

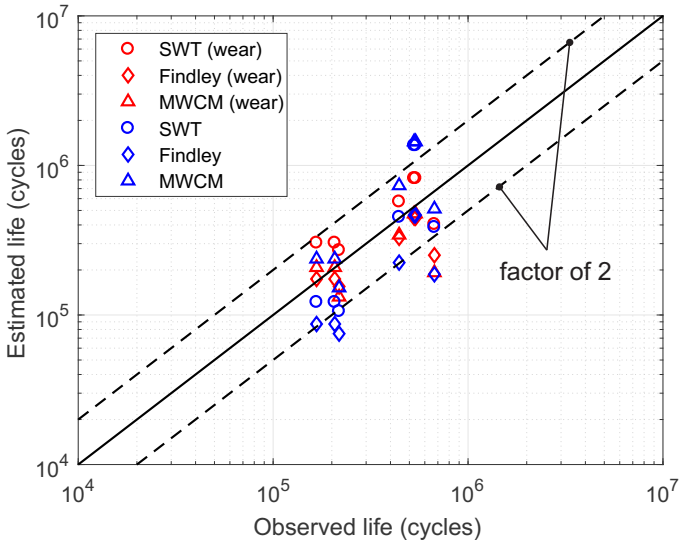


Figure 15: Estimated and observed fretting fatigue lives reported in [14, 16].

plain strain elements. Besides, as can be seen in the experimental results and as pointed out by [14, 16], the specimen thickness does not have a great influence in terms of life when the same levels of loads are considered. In other words, components subjected to the same stress gradients nearby the contact edges will experience similar lives despite the size of the slip areas.

Regarding the dispersion when evaluating fatigue lives, at a first glance, both predictions considering and neglecting wear effects seem reasonably accurate, Figure 15. Only a few cases lie outside the region defined by the factor of 2 lines. Besides, these cases are apparently more related to the multiaxial fatigue criterion used itself. In addition, Table 5 expresses the life estimate errors for each multiaxial fatigue criteria assessed in this work. In this setting, for the data here studied, when considering wear effects, the SWT model provided the least conservative results although all estimates had errors smaller 100 %. Findley and MWCM criteria lead to similar estimates, however with results a little more centred than the SWT ones and with a more conservative trend. On the other hand, when neglecting wear effects, estimates are in general more scattered than when considering wear. Additionally, except for tests T6 and consequently T7, where SWT and MWCM considerably overestimated the results, all other predictions got errors smaller than 100 %. Therefore, in spite of the results obtained considering wear effects are slightly better, neglecting wear does not seem to strongly affect multiaxial fatigue damage assessment still providing reasonable life predictions under partial slip conditions. Neglecting wear also simplifies the problem and significantly reduces its computational cost, which would be a key point if complex 3D components were being evaluated.

Table 5: Estimated errors considering (a) and neglecting wear effects (b).

| test | SWT | Findley | MWCM |
|---|---|---|---|
| **(a) Errors (%) considering wear:** | | | |
| T1 | 24 | -29 | -39 |
| T2 | 82 | 4 | 25 |
| T3 | -40 | -63 | -71 |
| T4 | 29 | -26 | -23 |
| T5 | 47 | -16 | 0 |
| T6 | 55 | -16 | -10 |
| T7 | 53 | -17 | -12 |
| **(a) Errors (%) neglecting wear:** | | | |
| T1 | -51 | -66 | -30 |
| T2 | -27 | -48 | 42 |
| T3 | -42 | -72 | -24 |
| T4 | 2 | -49 | 65 |
| T5 | -41 | -58 | 14 |
| T6 | 158 | -12 | 172 |
| T7 | 153 | -14 | 168 |
| *Erros (%) are defined as the difference between the estimated lives and the experimental ones divided by the experimental observations. | | | |

However, it is worth noting that, when considering wear effects, the fatigue damage tends to spread over a larger region and failure is predicted to happen inside the slip zone. For the load configuration T1, for example, failure is predicted close to the transition between the stick and the slip zone, Figure 16(a). On the other hand, when neglecting wear effects, failure is always predicted to take place near the contact trailing edge despite the load configuration assessed, Figure 16(b).

The author is aware that wear simulations carried out in this work did not take into account third body effects [52, 53] and variations of the friction coefficient [54]. Another important point is that, when performing wear simulations under partial slip conditions, cracks would have appeared at some point, and this would be responsible for modifying the contact stress distributions even more. However, in the view of the dispersion involved in fatigue, simplifications assumed in this work seem to be reasonable. It is also worth noting that, the material here considered was an aeronautical Ti-6Al-4V alloy, which has some interesting properties, for instance, high mechanical properties such as its hardness, corrosion resistance and fine surface finishing, which all along contributed to low wear rates [55]. In this setting, further investigations should also be employed to materials more susceptible to wear.

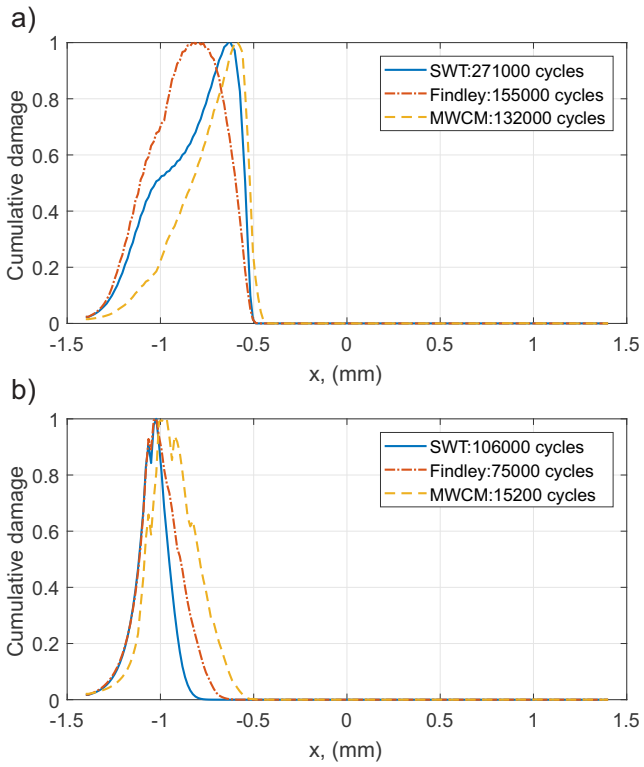


Figure 16: Damage distribution inward the contact at $L/2$ for the load configuration T1: (a) considering and (b) neglecting wear effects.

## 8. Conclusions

In this work, the influence of considering wear effects when estimating fretting fatigue life was investigated. Available fretting fatigue data for a Ti-6Al-4V alloy were confronted with both: life estimates taking into account the contact/stress evolution due to material removal and life estimates where these effects are neglected (simplifying approach often adopted). Numerical simulations were carried out through the FE method. Results have shown that, considering wear effects allow us to slightly improve the accuracy of life predictions, where results were less scattered when compared to estimates obtained when wear is disregarded. In order to estimate the fatigue life, the TCD has been used in association with three different multiaxial fatigue criteria (SWT, Findley and MWCM). When considering wear effects, all the models provided errors smaller than 85 % which is reasonable in terms of fatigue dispersion. Additionally, the SWT normal stress based criterion led to less conservative estimates when compared to Findley and MWCM approaches (shear stress based models). On the other hand, neglecting wear effects led to more scattered estimates. However, only for one of the 5 load configurations here assessed, SWT and MWCM multiaxial fatigue criteria provided errors around 160 %, while the other cases studied yielded errors less than 75 % in the estimates. In this setting, for the experimental data that one has assessed, i.e. fretting fatigue conditions under partial slip regime, neglecting wear effects in terms of material removal does not seem to strongly decrease the accuracy of life predictions, which on the other hand saves a lot of computational cost. Note that neglecting wear would not be the case for gross slip conditions where the high rate of wear induces the reduction of contact tractions and constantly removes severely damaged areas [12, 20].

## 9. Acknowledgements

Raphael A. Cardoso would like to acknowledge the scholarship granted by CAPES (Coordenação de Aperfeiçoamento de Pessoal de Nível Superior).

## Appendix A: Remeshing and adaptive meshing techniques applied to modelling wear

In this appendix, one gives more details concerning the implementation and numerical issues of the two different wear modelling strategies considered in this work. In this setting, Figure 17 displays a flowchart illustrating the FE-based wear model coupled with the remeshing technique. Herein, a main Python script manages all the process which consists in the simulation of each fretting cycle $i$ followed by the contact surfaces updating, where contact nodes are vertically moved according to Eq. (5) or (6) depending on the wear model used.

Figure 18, on the other hand, depicts the incremental wear simulation methodology when using the adaptive meshing (ALE adaptive meshing [29]). In this case, the main difference is that instead of computing the material removal

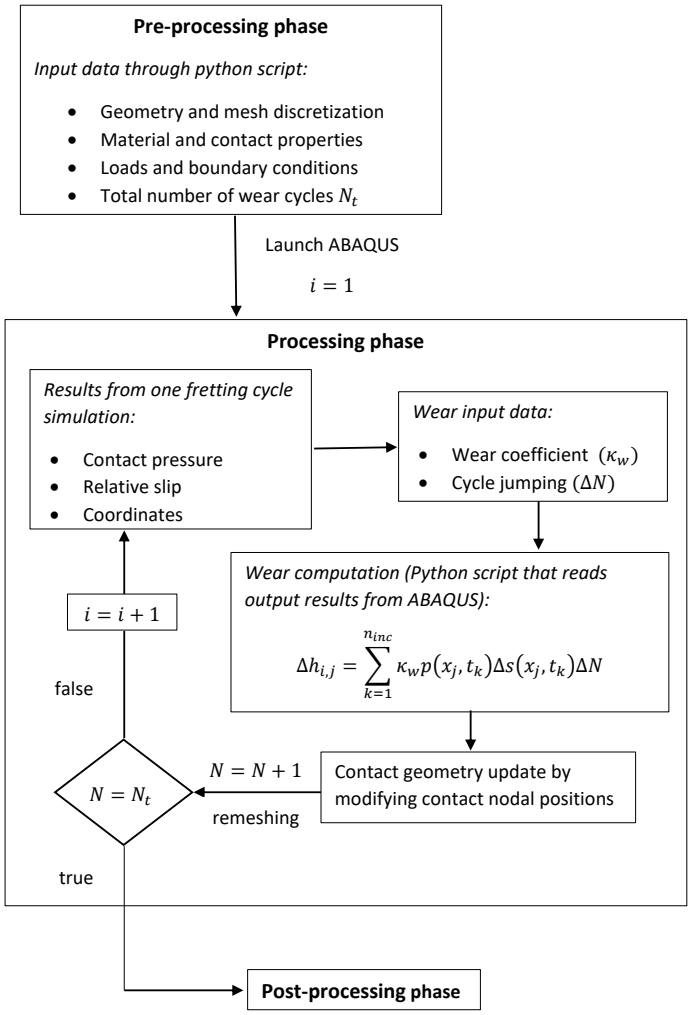


Figure 17: FE-based model for wear analysis using the remeshing technique.

and updating the contact surface at the end of a complete fretting cycle, wear calculation and contact nodes motion are carried out within a fretting cycle for each load increment. This procedure is implemented by a user subroutine (UMESHMOTION, [29]).

In order to evaluate these two methods, results from [10] were here reproduced and used as reference for validation. These authors have investigated the wear effects on the stress distribution under both partial and gross sliding conditions. Figure 19 depicts the geometry and load conditions considered, where first a normal load $P = 120$ N/mm is applied to the cylindrical pad pressing it onto the flat specimen which is fixed on the bottom surface. Then, while this normal load $P$ is held constant, a tangential oscillatory displacement $u_x$ is applied to the pad. The upper surface of the pad is also subjected to a multi-point constraint which prevents pad's rotation. Two different amplitudes of $u_x$ were investigated, a smaller one of 2.5 $\mu$m establishing partial slip conditions and larger one of 10 $\mu$m ensuring gross sliding regime.

The material considered was a high strength steel with Young modulus $E =$ 200 MPa, Poisson's ration $\nu = 0.3$ and a local wear coefficient $k_w = 1.0 \times 10^{-7}$ MPa$^{-1}$ [10]. The friction coefficient assumed in the simulations was $\mu = 0.6$.

Figure 20 shows the contact pressure distribution for different number of fretting cycles under partial slip conditions considering both contact surface update procedures (remeshing and adaptive meshing). In this case, the size of the mesh near the contacting surfaces was set equal to 5 $\mu$m. As can be seen, as the wear evolves, slip zones are worn out while the stick zone tends to support all external contact loads. For a high enough number of cycles (18000 cycles, Figure 20(a)), it is possible to observe that the pressure distributions along the initial slip zones are nearly null, which happens because these zones were completely removed at this point. In this case, a full stick condition is observed at the initial stick zone region where the pressure distribution is close to the one found in complete contact problems (flat-on-flat). Similar conclusions were obtained previously by [30] when evaluating wear effects under partial slip conditions analytically. This shifting of the hot spot zones from the contact edges towards the stick zones may explain why many times cracks are observed at the slip zones close the initial stick/slip zone region.

Results from Figure 20(a) were obtained by using the remeshing tehcnique and are in close agreement with the data provided by [10], which used a similar contact surface updating procedure. On the other hand, the adaptive mesh strategy overestimated wear effects. As can be seen in Figure 20(b), the size of the stick zone is always decreasing which consequently makes the peak pressure achieve very high values. Note as well that the pressure distribution at the initial slip zones falls to zero slower when compared to the remeshing technique. It may be due to the smoothing procedures performed on the ALE adaptive meshing algorithm [29]. However, this phenomenon only took place when partial slip conditions were evaluated, i.e. $u_x = 2.5$ $\mu$m.

When gross sliding conditions were assessed, both contact surface update procedures provided nearly the same results as depicted in Figure 21. In this case, the size of the mesh in the refined region surrounding the contact surfaces

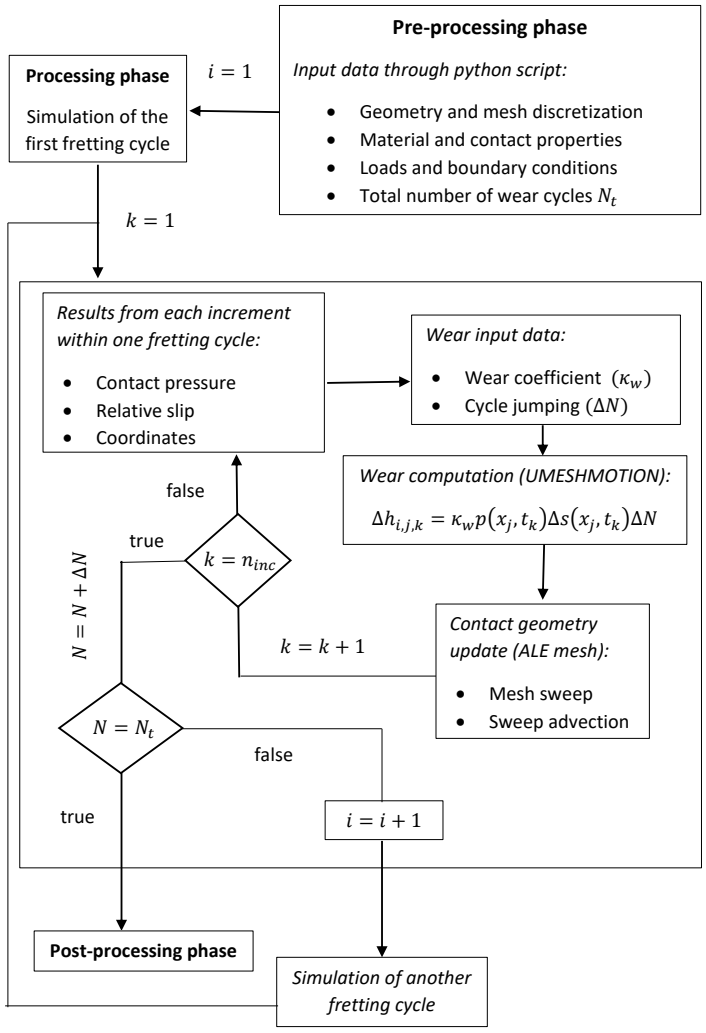


Figure 18: FE-based model for wear analysis using the ALE adaptive technique.

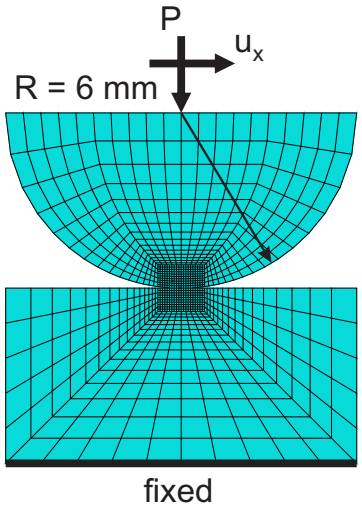


Figure 19: FE model used to validate wear implementations.

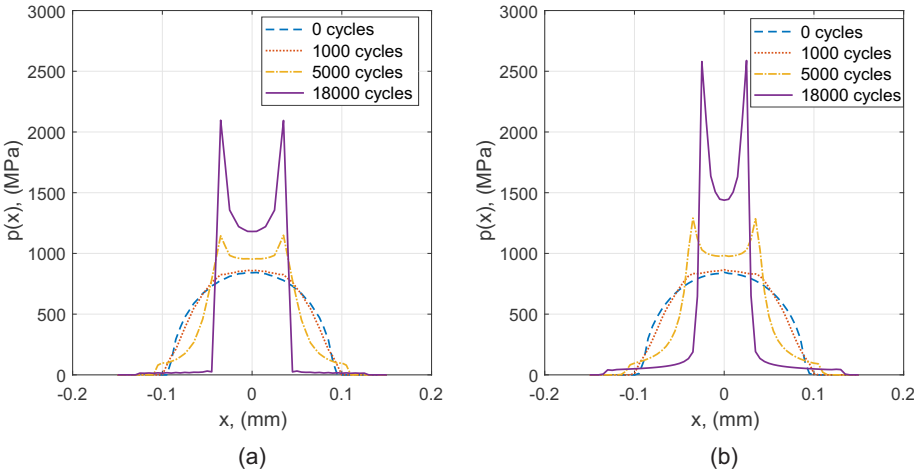


Figure 20: Contact pressure distributions under partial slip conditions ($P = 120$ N/mm, $u_x = 2.5$ $\mu$m, $R = 6$ mm) for different number of fretting cycles: (a) considering the remeshing technique and (b) the adaptive mesh.

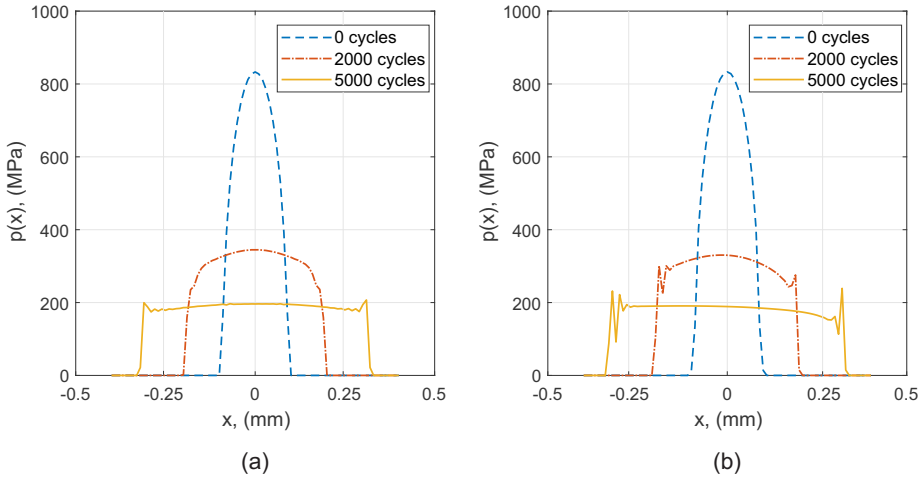


Figure 21: Contact pressure distributions under gross sliding conditions ($P = 120$ N/mm, $u_x = 10$ $\mu$m, $R = 6$ mm) for different number of fretting cycles: (a) considering the remeshing technique and (b) the adaptive mesh.

was defined equal to 10 $\mu$m. For the gross sliding regime, it is possible to see that, as the fretting cycles evolve, the contact region becomes larger and the pressure distribution tends to a flat distribution. Note that the initial peak pressure is around 4 times higher than that at 5000 fretting cycles. In addition, the large amount of material loss is constantly removing severely damaged areas, which hinders the propagation of cracks. Results depicted in Figure 21 are in very good accordance with the ones presented by [10]. Results from Figures 20 and 21 were obtained before start applying the tangential displacement to the pad ($u_x = 0$).

For the partial slip conditions, a jumping cycle ($\Delta N$) of 2000 was used when using the adaptive meshing procedure. For the remeshing technique, the jumping cycle was set to 500. Fretting cycles were equally divided into 16 steps when using the remeshing technique and 50 steps when using the adaptive meshing for the partial slip regime. For gross sliding conditions, the jumping cycle was set to 25 and 100, respectively, when using the remeshing and adaptive meshing procedures. In this case, for the fretting cycle increments, 16 time steps were used for the remeshing approach while 100 time steps for the adaptive meshing one.

Generally speaking, the ALE adaptive meshing is computationally more efficient and allows the use of higher cycle jumps. This procedure permits the modification of the contact surface incrementally throughout a tangential cycle. In addition, the unloading and loading phases of the normal load does not need to be carried out as it is done in the remeshing technique. However, this strategy is more memory demanding once all the fretting cycles incrementation data need to be stored in memory while the FE analysis is running, which can be

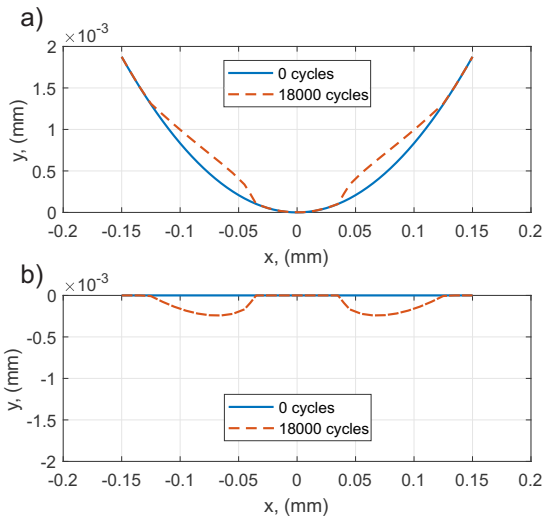


Figure 22: Worn profile under partial slip conditions ($P = 120$ N/mm, $u_x = 2.5$ $\mu$m, $R = 6$ mm): (a) pad, (b) specimen.

a huge drawback when considering large problems. Besides, the apparently no stabilization of the worn profile under partial slip conditions is a considerable shortcoming in the scope of this work, once high cycle fretting fatigue cases will be evaluated. Therefore, the remeshing technique was chosen in order to update contact surfaces when performing fretting simulations in this work. Figures 22 and 23 show the worn profile of the flat specimen and the cylindrical pad by using the remeshing technique for both slip regimes.

It is worth noting that, in spite of the slip regime, [11] obtained good results by estimating the effect of slip amplitude on fretting fatigue life by using the adaptive meshing technique. In this case, good results under partial slip conditions may be explained due to the fact that, for the data assessed by them, contact loads and wear coefficient were smaller, which consequently decreases wear rates. And as can be seen in Figure 22, for the first 5000 cycles, results obtained by using the remeshing or the adaptive meshing technique do not diverge too much. In other words, for a certain level of wear, under partial partial slip conditions, both procedures provide similar results.

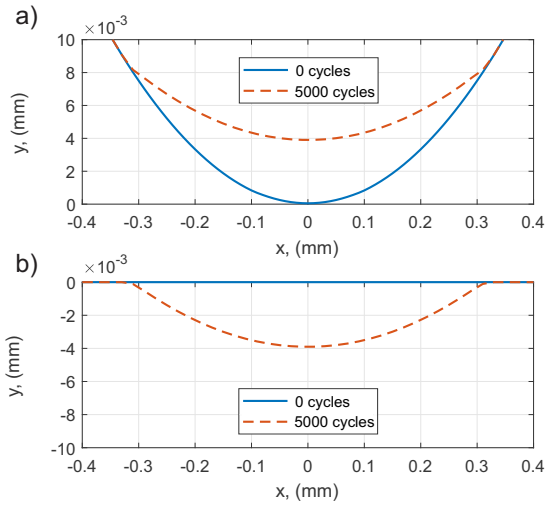


Figure 23: Worn profile under gross sliding conditions ($P = 120$ N/mm, $u_x = 10$ $\mu$m, $R = 6$ mm): (a) pad, (b) specimen.

## References


[1] G. Spink, Fretting fatigue of a 212% nicrmov low pressure turbine shaft steelthe effect of different contact pad materials and of variable slip amplitude, Wear 136 (2) (1990) 281–297.

[2] T. Lindley, Fretting fatigue in engineering alloys, International journal of fatigue 19 (93) (1997) 39–49.

[3] J. A. Araujo, D. Nowell, The effect of rapidly varying contact stress fields on fretting fatigue, International Journal of Fatigue 24 (7) (2002) 763–775.

[4] T. Hattori, M. Nakamura, T. Watanabe, Simulation of fretting-fatigue life by using stress-singularity parameters and fracture mechanics, Tribology international 36 (2) (2003) 87–97.

[5] J. A. Araujo, D. Nowell, R. C. Vivacqua, The use of multiaxial fatigue models to predict fretting fatigue life of components subjected to different contact stress fields, Fatigue & Fracture of Engineering Materials & Structures 27 (10) (2004) 967–978.

[6] C. Navarro, S. Muñoz, J. Dominguez, On the use of multiaxial fatigue criteria for fretting fatigue life assessment, International Journal of fatigue 30 (1) (2008) 32–44.

[7] J. A. Araújo, L. Susmel, M. S. T. Pires, F. C. Castro, A multiaxial stress-based critical distance methodology to estimate fretting fatigue life, Tribology International 108 (2017) 2–6.

[8] R. Cardoso, E. d. S. Campos, J. Ferreira, D. Wang, J. Araújo, A crack arrest methodology based on bazants parameter to fretting fatigue, Theoretical and Applied Fracture Mechanics 95 (2018) 208–217.

[9] I. R. McColl, J. Ding, S. B. Leen, Finite element simulation and experimental validation of fretting wear, Wear 256 (11-12) (2004) 1114–1127.

[10] J. Ding, S. B. Leen, I. R. McColl, The effect of slip regime on fretting wear-induced stress evolution, International journal of fatigue 26 (5) (2004) 521–531.

[11] J. J. Madge, S. B. Leen, I. R. McColl, P. H. Shipway, Contact-evolution based prediction of fretting fatigue life: effect of slip amplitude, Wear 262 (9-10) (2007) 1159–1170.

[12] J. J. Madge, S. B. Leen, P. H. Shipway, The critical role of fretting wear in the analysis of fretting fatigue, Wear 263 (1-6) (2007) 542–551.

[13] I. I. Argatov, X. Gómez, W. Tato, M. A. Urchegui, Wear evolution in a stranded rope under cyclic bending: Implications to fatigue life estimation, Wear 271 (11-12) (2011) 2857–2867.

[14] B. Ferry, Study of the stress gradient effect and the size effect in fretting fatigue., Ph.D. thesis, Université Paris-Saclay and University of Brasilia (2017).

[15] B. Ferry, J. A. Araújo, S. Pommier, K. Demmou, Life of a ti–6al–4v alloy under fretting fatigue: Study of new nonlocal parameters, Tribology International 108 (2017) 23–31.

[16] J. A. Araujo, B. Ferry, C. Montebello, J. Meriaux, S. Pommier, Study of size effects in fretting fatigue, (under publication).

[17] S. Hannel, S. Fouvry, P. Kapsa, L. Vincent, The fretting sliding transition as a criterion for electrical contact performance, Wear 249 (9) (2001) 761–770.

[18] Z. R. Zhou, L. Vincent, Mixed fretting regime, Wear 181 (1995) 531–536.

[19] O. Vingsbo, S. Söderberg, On fretting maps, Wear 126 (2) (1988) 131–147.

[20] S. Garcin, S. Fouvry, S. Heredia, A fem fretting map modeling: Effect of surface wear on crack nucleation, Wear 330 (2015) 145–159.

[21] S. Fouvry, T. Liskiewicz, P. Kapsa, S. Hannel, E. Sauger, An energy description of wear mechanisms and its applications to oscillating sliding contacts, Wear 255 (1-6) (2003) 287–298.

[22] T. Doca, F. M. A. Pires, Finite element modeling of wear using the dissipated energy method coupled with a dual mortar contact formulation, Computers & Structures 191 (2017) 62–79.

[23] J. F. Archard, Contact and rubbing of flat surfaces, Journal of applied physics 24 (8) (1953) 981–988.

[24] A. Palmgren, Die lebensdauer von kugellagern, Zeitshrift des Vereines Duetsher Ingenieure 68 (1924) 339–341.

[25] M. A. Miner, Cumulative damage in fatigue, Journal of Applied Mechanics 12 (1945) A159–A164.

[26] J. J. Madge, Numerical modelling of the effect of fretting wear on fretting fatigue, Ph.D. thesis, University of Nottingham (2009).

[27] A. Cruzado, S. B. Leen, M. A. Urchegui, X. Gómez, Finite element simulation of fretting wear and fatigue in thin steel wires, International Journal of Fatigue 55 (2013) 7–21.

[28] M. Z. Silva, Estudo da influência do desgaste na falha prematura de componentes de linhas de ancoragem, Master's thesis, University of Brasilia (2016).

[29] Abaqus, ABAQUS User's Manuals, Version 6.13, Dassault Systemes Simulia Corp, 2013.

[30] M. Ciavarella, D. A. Hills, Brief note: Some observations on oscillating tangential forces and wear in general plane contacts, European Journal of Mechanics-A/Solids 18 (3) (1999) 491–497.

[31] H. J. Gough, H. V. Pollard, The strength of metals under combined alternating stresses, Proceedings of the institution of mechanical engineers 131 (1) (1935) 3–103.

[32] H. J. Gough, Engineering steels under combined cyclic and static stresses, Proceedings of the Institution of Mechanical Engineers 160 (1) (1949) 417–440.

[33] W. N. Findley, A theory for the effect of mean stress on fatigue of metals under combined torsion and axial load or bending, no. 6, Engineering Materials Research Laboratory, Division of Engineering, Brown University, 1958.

[34] R. N. Smith, P. Watson, T. H. Topper, A stress-strain parameter for the fatigue of metals, Journal of Materials 5 (4) (1970) 767–788.

[35] L. Susmel, P. Lazzarin, A bi-parametric wöhler curve for high cycle multiaxial fatigue assessment, Fatigue & Fracture of Engineering Materials & Structures 25 (1) (2002) 63–78.

[36] A. Carpinteri, M. de Freitas, A. Spagnoli, The influence of static mean stresses applied normal to the maximum shear planes in multiaxial fatigue, Biaxial/Multiaxial Fatigue and Fracture 31 (2003) 123.

[37] L. Susmel, Multiaxial fatigue limits and material sensitivity to non-zero mean stresses normal to the critical planes, Fatigue & Fracture of Engineering Materials & Structures 31 (3-4) (2008) 295–309.

[38] L. Susmel, Multiaxial notch fatigue, Elsevier, 2009.

[39] D. Taylor, Geometrical effects in fatigue: a unifying theoretical model, International Journal of Fatigue 21 (5) (1999) 413–420.

[40] M. H. El Haddad, K. N. Smith, T. H. Topper, Fatigue crack propagation of short cracks, Journal of Engineering Materials and Technology 101 (1) (1979) 42–46.

[41] L. Susmel, D. Taylor, et al., Can the conventional high-cycle multiaxial fatigue criteria be re-interpreted in terms of the theory of critical distances, Structural Durability & Health Monitoring 2 (2) (2006) 91–108.

[42] C. Montebello, S. Pommier, K. Demmou, J. Leroux, J. Meriaux, Analysis of the stress gradient effect in fretting-fatigue through nonlocal intensity factors, International Journal of Fatigue 82 (2016) 188–198.

[43] J. Bellecave, S. Pommier, Y. Nadot, J. Meriaux, J. A. Araújo, T-stress based short crack growth model for fretting fatigue, Tribology International 76 (2014) 23–34.

[44] K. Le Biavant-Guerrier, Etude de l'amorçage de fissures de fatigue dans le ti-6al-4v, Ph.D. thesis, Ecole Centrale Paris (2000).

[45] H. Hertz, Über die berührung fester elastischer körper., Journal für die reine und angewandte Mathematik 92 (1882) 156–171.

[46] C. Cattaneo, Sul contatto di due corpi elastici: distribuzione locale degli sforzi, Rend. Accad. Naz. Lincei 27 (6) (1938) 342–348.

[47] R. D. Mindlin, Compliance of elastic bodies in contact, J. appl. Mech. 16 (1949) 259–268.

[48] A. R. Kallmeyer, A. Krgo, P. Kurath, Evaluation of multiaxial fatigue life prediction methodologies for ti-6al-4v, Journal of engineering materials and technology 124 (2) (2002) 229–237.

[49] E. N. Mamiya, J. A. Araújo, F. C. Castro, Prismatic hull: a new measure of shear stress amplitude in multiaxial high cycle fatigue, International Journal of Fatigue 31 (7) (2009) 1144–1153.

[50] J. A. Araújo, L. Susmel, D. Taylor, J. C. T. Ferro, E. N. Mamiya, On the use of the theory of critical distances and the modified wöhler curve method to estimate fretting fatigue strength of cylindrical contacts, International Journal of Fatigue 29 (1) (2007) 95–107.

[51] D. Taylor, Applications of the theory of critical distances in failure analysis, Engineering Failure Analysis 18 (2) (2011) 543–549.

[52] J. Ding, I. R. McColl, S. B. Leen, P. H. Shipway, A finite element based approach to simulating the effects of debris on fretting wear, Wear 263 (1-6) (2007) 481–491.

[53] S. Basseville, E. Héripré, G. Cailletaud, Numerical simulation of the third body in fretting problems, Wear 270 (11-12) (2011) 876–887.

[54] T. Yue, M. A. Wahab, Finite element analysis of fretting wear under variable coefficient of friction and different contact regimes, Tribology International 107 (2017) 274–282.

[55] R. B. Waterhouse, Fretting wear in asm handbook, friction lubrication, and wear thecnology, ASM International 18 (1992) 242–256.